

# Confocal fluorescence microendoscopy of bronchial epithelium

**Pierre M. Lane**

**Stephen Lam**

**Annette McWilliams**

**Jean C. leRiche**

British Columbia Cancer Research Center  
Cancer Imaging Department  
675 West 10th Avenue  
Vancouver, BC V5Z 1 L3  
Canada

**Marshall W. Anderson**

University of Cincinnati  
Molecular Oncogenesis  
Cincinnati, Ohio 45267

**Calum E. MacAulay**

British Columbia Cancer Research Center  
Cancer Imaging Department  
675 West 10th Avenue  
Vancouver, BC V5Z 1 L3  
Canada

**Abstract.** Confocal microendoscopy permits the acquisition of high-resolution real-time confocal images of bronchial mucosa via the instrument channel of an endoscope. We report here on the construction and validation of a confocal fluorescence microendoscope and its use to acquire images of bronchial epithelium *in vivo*. Our objective is to develop an imaging method that can distinguish preneoplastic lesions from normal epithelium to enable us to study the natural history of these lesions and the efficacy of chemopreventive agents without biopsy removal of the lesion that can introduce a spontaneous regression bias. The instrument employs a laser-scanning engine and bronchoscope-compatible confocal probe consisting of a fiber-optic image guide and a graded-index objective lens. We assessed the potential of topical application of physiological pH cresyl violet (CV) as a fluorescence contrast-enhancing agent for the visualization of tissue morphology. Images acquired *ex vivo* with the confocal microendoscope were first compared with a bench-top confocal fluorescence microscope and conventional histology. Confocal images from five sites topically stained with CV were then acquired *in vivo* from high-risk smokers and compared to hematoxylin and eosin stained sections of biopsies taken from the same site. Sufficient contrast in the confocal imagery was obtained to identify cells in the bronchial epithelium. However, further improvements in the miniature objective lens are required to provide sufficient axial resolution for accurate classification of preneoplastic lesions. © 2009 Society of Photo-Optical Instrumentation Engineers. [DOI: 10.1117/1.3103583]

Keywords: Confocal; microendoscopy; endomicroscopy; lung cancer; fluorescence; *in vivo*; cresyl violet.

Paper 08232RR received Jul. 14, 2008; revised manuscript received Jan. 8, 2009; accepted for publication Jan. 9, 2009; published online Mar. 31, 2009.

## 1 Introduction

In the United States and Canada, lung cancer accounts for 28% of all cancer deaths. There are more patients who die from lung cancer than from breast, colon, and prostate cancers combined.<sup>1</sup> The overall five-year survival rate of lung cancer is 16%.<sup>1</sup> Unfortunately, advances in the detection and treatment of this disease have not resulted in a significant improvement in mortality rates. In the last 50 years, lung-cancer incidence increased by 249% and the mortality by 259%.<sup>2</sup>

Approximately 85% of all lung cancers are related to tobacco smoking. Currently, there are approximately 45 million former smokers in the U.S. Approximately half of all the newly diagnosed lung-cancer cases are now former smokers.<sup>3</sup> Alternative cancer-control strategies such as chemoprevention need to be developed to reduce lung-cancer mortality, especially for smokers who have followed medical advice to give up smoking. Chemoprevention refers to the use of pharmacologic or natural agents that inhibit the development of inva-

sive cancer either by blocking the DNA damage that initiates carcinogenesis or by arresting or reversing the progression of intraepithelial neoplasia in which such damage has already occurred.<sup>4</sup> Chemoprevention relies on the concept that epithelial cancers do not arise as the result of a single initiating event but rather represent a multistep process characterized by a period that is often 20 years or more between the initiation event and the onset of invasive or metastatic disease. The disease to be treated is not cancer but the process of carcinogenesis. Before embarking on expensive and long Phase III trials, potentially active chemopreventive agents are tested in Phase II trials using intermediate endpoint biomarkers such as bronchial dysplasia. We have previously reported that although the prevalence of mild dysplasia may decline on smoking cessation, the prevalence of high-grade dysplasia and carcinoma *in situ* are similar in current and former smokers.<sup>5</sup> Attempts have been made to study the natural history of precancerous bronchial lesion.<sup>6</sup> Mechanical removal of the lesions with the biopsy procedure has been implicated as a contributing factor to the apparently high spontaneous regression rate of dysplastic lesions in chemoprevention trials<sup>7</sup> due to the

Address all correspondence to: Pierre M. Lane, British Columbia Cancer Research Center Cancer Imaging Department, 675 West 10th Avenue, Vancouver, BC V5Z 1L3. Tel. (604) 675-8087; Fax. (604) 675-8099; E-mail: plane@bccrc.ca.

small size of these lesions.<sup>8</sup> Park et al. have estimated the size of molecularly abnormal clonal patches in normal or slightly abnormal bronchial epithelium of patients with lung cancer to be <0.5 mm.<sup>9</sup> The dimensions of a tissue patch removed using standard biopsy forceps is typically 1–2 mm in size and therefore is often larger than the lesion. The primary objective of this study was to develop an imaging method that can distinguish preneoplastic lesions from normal epithelium to enable us to study the natural history of these lesions and the efficacy of chemopreventive agents without mechanical removal of the lesion that can introduce a spontaneous regression bias.

Although it is possible to obtain confocal reflectance and fluorescence images from endogenous contrast mechanisms, the use of exogenous contrast agents simplifies the optical instrumentation, improves the signal-to-noise ratio (sensitivity) of the images, and can offer increased specificity especially if contrast agents are chosen to target particular molecules. The obvious disadvantage is that the contrast agent must be easily administered, inexpensive, and nontoxic to humans.

Cresyl violet (CV) is used clinically as an absorptive coloring agent in combination with indigo carmine during chromoendoscopy to accentuate the colonic mucosal features.<sup>10</sup> Chromoendoscopy involves the topical application of stains or pigments to improve tissue localization, characterization, or diagnosis during endoscopy. The dye preferentially stains the margins of the pits to achieve superior visualization of the contours of the colonic folds. Magnification endoscopy (35–100 times magnification) in conjunction with CV staining permits near-microscopic visualization through an endoscope and is the basis of the diagnostic technique known as pit-pattern classification for mucosal abnormalities in the colon.<sup>10</sup> CV has traditionally been used as an absorptive stain; however, it also produces a red fluorescent signal that can be easily detected. George and Meining investigated CV as a fluorescence contrast agent for *in vivo* histopathology.<sup>11</sup> Recently, Meining et al. demonstrated the potential of confocal microscopy to diagnose neoplasia during endoscopy of the upper and lower gastrointestinal tract using CV as a fluorescence contrast agent.<sup>12</sup> However, native CV is acidic. Instilling acidic fluid in the lung can result in noncardiogenic pulmonary edema that can be fatal. We report here the first use of physiologic pH-CV as a fluorescent contrast agent for confocal microendoscopy of the bronchial mucosa.

## 2 Materials and Methods

### 2.1 Staining Protocol

The CV fluorescent stain was prepared based on the protocol described by George and Meining.<sup>11</sup> CV acetate (C1791, Sigma-Aldrich) was dissolved in phosphate-buffered saline (PBS) at a concentration of 1% (w/v). The solution was filtered using a 0.2  $\mu\text{m}$  pore-size sterilization filter (524-0020, Nalgene) to remove bacteria and any undissolved solute. A second CV stain with neutral pH was prepared by adding 1 M sodium hydroxide to a fraction of the original (acidic) CV stain from the previous step. These stains were tested in cultured cells and bronchial biopsy specimens *ex vivo*. Only physiological pH-CV was used *in vivo* by topical application in the bronchial surface.

### 2.2 Bench-Top Microscopes

Wide-field fluorescence and confocal fluorescence microscopy were performed on a Carl Zeiss Axioskop 2 mot using a 25X/0.80 water-immersion objective lens. Fluorescence images were acquired using excitation light at 545 nm from an arc lamp (X-Cite 120, Mississauga, ON), and emission light was collected at 610 nm (41002b filter set, Chroma Technology, Rockingham, VT). Images were captured using a charge-coupled device (CCD) camera (PMI 1400, QImaging, Surrey, BC). Confocal fluorescence microscopy was performed on the same Zeiss microscope platform using a custom-built confocal attachment. The microscope attachment, which employs a digital micromirror device [(DMD), Texas Instruments] for scanning,<sup>13</sup> has been described previously.<sup>14,15</sup> The DMD scans a pattern of several thousand diffraction-limited spots over the field of view in a raster pattern. The in-focus and out-of-focus light from each spot is detected with the CCD camera, processed, and finally assembled into a confocal image.

Hematoxylin and eosin (H&E) stained sections of bronchial biopsies were photographed on a Nikon Eclipse using a 10X/0.45 microscope objective. Color images were recorded using a CCD camera (MicroPublisher 3.3, QImaging). All H&E images were stretched by a factor of 2 (in the *x* and *y* directions) to compensate for tissue shrinkage introduced by formalin fixation and staining. Our measurements of bronchial epithelial thickness acquired *in vivo* using optical coherence tomography (OCT)<sup>16</sup> and postbiopsy from similar H&E sections (unpublished data) indicate 50% shrinkage due to tissue processing. This value is consistent with shrinkage reported in a hamster cheek-pouch model of carcinogenesis<sup>17</sup> and resected human colorectal specimens.<sup>18</sup>

### 2.3 Confocal Microendoscope

The confocal microendoscope consists of a custom-built laser-scanning confocal engine and miniature probe designed to be used through the instrumentation channel of a standard bronchoscope. The instrument employs a fiber-optic image guide, and scanning is accomplished at the proximal end of the image guide by the laser-scanning confocal engine.

The confocal engine is based on conventional laser-scanning. Two design forms have been reported in the literature,<sup>19</sup> and both are available commercially. The first employs a scanner proximal to a fiber-optic image guide,<sup>20,21</sup> while the second uses a miniaturized scanner distal to a single optical fiber.<sup>22,23</sup> A proximal-scanning device is available from Mauna Kea Technologies (Paris, France), while an instrument based on distal scanning, developed in collaboration with Optiscan (Victoria, Australia), is available from Pentax (Montvale, NJ). The design form of the instrument reported in this contribution is similar to that of Mauna Kea Technologies and employs a resonance scanner proximal to a fiber-optic image guide. A block diagram of the system is shown in Fig. 1. The system uses a 15-mW yellow laser at 561 nm (85 YCA 015, Melles Griot). The beam is spatially filtered and expanded before entering the filter-block assembly. The filter block employs a 580-nm dichroic mirror (z561rdc, Chroma Technology) and a 580 nm long-pass (HQ5801p, Chroma Technology) emission filter. Excitation light from the filter block is scanned by a resonant scanner (CRS, GSI Group,

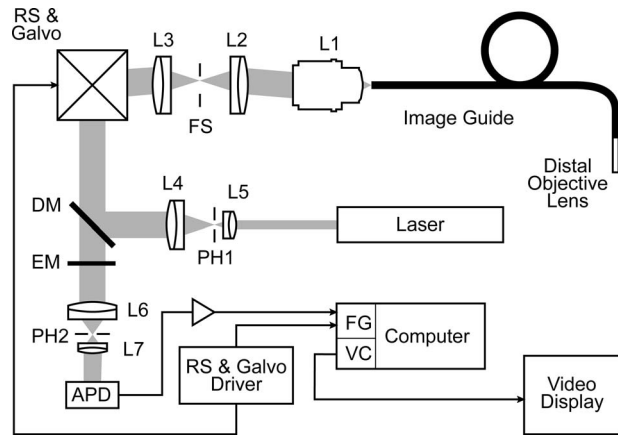


**Fig. 1** Block diagram of the confocal microendoscope system. Illumination pinhole (PH1); dichroic mirror (DM); resonance scanner (RS); field stop (FS); microscope objective lens (L1); emission filter (EM); detection pinhole (PH2); avalanche photodiode (APD); frame grabber (FG); video card (VC).

Bedford, MA) and galvanometer (VM500, GSI Group) mounted in mutually orthogonal axes at close proximity. The center-of-rotation of the scanning mirror pair is projected into the back pupil plane of a Nikon 20X/0.75 multi-immersion objective lens. The proximal end of the image guide is placed at the focal plane of the microscope objective lens. The image guide is optically coupled to the objective lens using index-matching oil with a refractive index of 1.4920 (Cargille Laboratories, Cedar Grove, NJ) to match closely that of the fiber cores in the image guide to reduce the optical loss due to Fresnel reflections. Fluorescent light is collected from the image guide by the objective lens, descanned, and projected through the filter-block assembly onto a detection pinhole. The size of the detection pinhole is easily adjusted. Light passing through the detection pinhole is collected by an avalanche photodiode [(APD), C5460, Hamamatsu, Bridgewater, NJ].

The signal from the APD is amplified and then digitized by a frame grabber (Meteor II, Matrox, Dorval, QC) using synchronization signals derived from the resonant scanner. The 4-kHz fast-axis (horizontal) scan frequency is determined by the resonance scanner. There are 526 scan lines per frame (512 active and 14 retrace), resulting in a frame rate of  $\sim 7$  Hz. Each scan line is digitized as 1024 points and then interpolated into 512 points using a look-up table to correct for the nonuniform spatial sampling introduced by the sinusoidal velocity of the resonance scanner. Raw-image sequences ( $1024 \times 512$  at 7 fps) are displayed and saved directly to hard disk in real time. The raw-image sequences were processed off-line using MATLAB to produce audio-video-interleaved format movies ( $512 \times 512$  at 7 fps). The off-line processing includes interpolation (as described above), spatial filtering to reduce the fiber pattern generated by the image guide, and contrast stretching.

The confocal probe consists of a fiber-optic image guide with a distal graded-index (GRIN) objective lens. A schematic diagram of the probe is illustrated in Fig. 2. The field-of-view of the image guide (FIGH-30-650S, Fujikura) is  $600 \mu\text{m}$  and is composed of 30,000 individual fibers with an NA of 0.35.

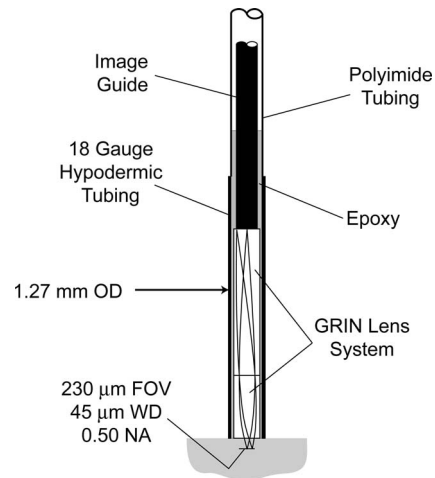


**Fig. 2** Schematic diagram of the confocal probe. The magnification from tissue to image guide is 2.6 times.

The objective lens is a 2.6X/0.5 numerical aperture (NA) saline immersion objective (Grintech GmbH, Jena Germany) assembled from two back-to-back GRIN lenses.<sup>24</sup> The lens assembly is bonded to the distal end of the image guide using a UV-curing adhesive. The objective lens assembly and lens-fiber interface is epoxied into a 10 mm length of 18 gauge (1.27 mm diameter) stainless steel tubing for mechanical protection. The remainder of the image guide is protected by polyamide tubing. The proximal end of the image guide was terminated with a sub-miniature A (SMA) fiber connector to facilitate the removal and installation of different probes.

#### 2.4 Lateral and Axial Resolution

The optical resolution of the confocal microendoscope probe was characterized by imaging calibration targets. As reported previously,<sup>25</sup> the lateral resolution of the confocal probe was 360 lp/mm ( $1.4\text{-}\mu\text{m}$  features) and was limited by the size of the optical fibers as projected into the tissue through the GRIN objective lens.

The axial resolution of the system is limited by the chromatic aberration introduced by the GRIN lens objective. The axial chromatic aberration was determined experimentally by measuring the working distance in water using green-yellow light at 560 nm (excitation wavelength) and then using red light at 630 nm (peak emission wavelength of CV when excited at 560 nm). The working distance was  $39 \mu\text{m}$  at 560 nm and  $49 \mu\text{m}$  at 630 nm, resulting in substantial axial chromatic aberration. In fact, the Stokes shift of 70 nm due to the CV fluorescence results in a focal shift of  $10 \mu\text{m}$ .

Characterization of this lens system and image guide by our group<sup>25</sup> and others<sup>24</sup> has shown an axial full width at half-maximum (fwhm) resolution of  $16 \mu\text{m}$  under monochromatic illumination at 633 nm. The axial resolution of the system was not measured in fluorescence mode; however, it can be approximated as the sum of the monochromatic axial resolution and the axial chromatic aberration introduced by the Stokes shift. Using the approximation, the axial fwhm resolution is  $26 \mu\text{m}$ .

Although the chromatic aberration of the GRIN lens system significantly impaired the axial resolution of the system,

it also had a large impact on its optical efficiency. The ellipsoidal excitation and emission volumes (each approximately  $16 \times 3 \times 3 \mu\text{m}$ ) were separated along the optical axis by  $10 \mu\text{m}$ , resulting in little spatial overlap. Consequently, the confocal detection pinhole had to be quite large in order to collect enough light. However, even at this degree of confocality, the images have sufficient sectioning to capture tissue architecture.

## 2.5 Imaging of Cultured Cells

Images of cultured cells were acquired to determine whether the staining properties of a 1% CV solution were effected by neutralizing its pH. Cervical-cancer (SiHa) cells from the American Type Culture Collection (HTB35) were cultured on glass slides covered with growth medium. We used cervical epithelial cells as a surrogate for lung-cancer cells because at the time, this was the only cell type available in our lab and we were only using the cells to assess the effect of changes in pH of CV on the fluorescence yield from cells. Two slides were stained topically and then washed in PBS, one with the native (acidic) 1% CV solution and the other with the pH-adjusted 1% CV solution. A third slide of cells was not stained as a control. The incubation time for the native and pH-adjusted stains was 120 s. The slides were imaged in transmission and wide-field fluorescence, and the difference in emitted fluorescence intensity was measured.

The cellular fluorescence after the application of CV with different pH was calculated by averaging the pixel intensity over the entire cell. The mean and standard deviation of cellular fluorescence for a population of cells contained in the center of a single field of view ( $>50$  cells) was calculated to describe the cellular fluorescence of the particular stain preparation.

The rate of CV uptake in cultured cells was determined using the confocal probe to acquire a time course of images starting immediately after the topical application of the CV solution. This experiment employed normal human bronchial epithelial (NHBE) cells from Lonza Walkersville, Inc., cultured directly on slides and stained topically with pH-adjusted 1% CV solution as described above. Cultures of NHBE cells were grown on six slides, and each slide was incubated in CV for a different time interval. In sequence, each cell culture was topically stained, incubated for 4, 8, 16, 30, 60, or 120 s, washed with PBS, and then imaged.

## 2.6 Ex Vivo Imaging of Bronchial Biopsy Specimens

Bronchial biopsies were obtained from participants in two National Institute of Health (NIH)-funded lung-cancer chemoprevention trials (P01-CA096964 and U01-CA96109). Informed consent was obtained in all participants. The protocol was approved by the Review of Ethics Board of the British Columbia Cancer Agency and the University of British Columbia.

Immediately following biopsy, the fresh specimens were placed in a Petri dish on a small piece of PBS-moistened sterile surgical gauze and then transported to the imaging lab. The biopsies were stained in the pH-adjusted 1% CV solution for 120 s and then gently washed in PBS. The stained biopsies were placed in shallow 2-in.-diam well dishes and hydrated with additional PBS. The epithelial surface of the bi-

opsies (luminal wall of the bronchial passageway) was oriented to face the objective lens such that *en face* images were acquired. Orientation of the epithelium was facilitated by identifying the green autofluorescence of the stroma when the sample was illuminated with blue light. A cover glass was placed on specimens imaged using the bench-top microscope to prevent the biopsy from adhering to the objective lens. The specimens imaged using the confocal probe were not cover slipped. Imaging was completed within 2 h of tissue removal.

One of the seven biopsy specimens was imaged in fluorescence using both the bench-top confocal microscope and the miniature confocal microendoscopy probe to determine the image quality that could be achieved with the endoscopic probe compared to a bench-top confocal microscope. After fluorescence imaging, all the biopsy specimens were fixed in buffered formalin, paraffin embedded, and stained using H&E as per standard protocols for histopathological classification by an experienced lung pathologist (JCL). Because it was unknown whether the CV staining procedure would affect the histopathological diagnosis of the samples used in this study, two biopsies were acquired at each site and only one biopsy was stained with CV prior to histopathology examination.

## 2.7 In Vivo Imaging

Confocal microendoscopy was performed in conjunction with conventional fluorescence bronchoscopy on five patients at the BC Cancer Agency in February and March of 2006. All five patients were enrolled in existing NIH-funded chemoprevention trials (P01-CA096964 and U01-CA96109). Informed consent was obtained in all participants. The protocol was approved by the Review of Ethics Board of the British Columbia Cancer Agency and the University of British Columbia.

The procedure for confocal microendoscopy was added to the existing clinical trial protocol for fluorescence bronchoscopy directed bronchial biopsies. The participants first underwent fluorescence bronchoscopy using an Olympus BF-40 bronchoscope and Xillix LIFE-Lung system.<sup>26</sup> On completion of the fluorescence bronchoscopy, the pH-adjusted CV solution was instilled topically using either a spray catheter or a brush-biopsy sheath via the biopsy channel of the bronchoscope to the sites to be imaged using the confocal microendoscope. We did not wash the surface afterward, as the subject usually removed the CV not taken up by the cells during spontaneous breathing and coughing. The BF-40 bronchoscope was then removed and a second bronchoscope (Olympus BF-XT40) with a larger instrument channel was inserted to perform the confocal microendoscopy. The second bronchoscope was navigated to the site(s) that had been stained previously, and the confocal probe was inserted down the instrument channel and brought into physical contact with the site of interest. The time interval between topical application of the stain and insertion of the larger channel bronchoscope to the same site was typically about 120 s. Short confocal videos were acquired at each site. After the completion of the confocal imaging, the confocal microendoscopy and the BF-XT40 bronchoscope were removed and the remainder of the clinical bronchoscopy procedure was completed using the BF-40 bronchoscope. Biopsy of the sites of interest was performed under autofluorescence bronchoscopy guidance. Be-

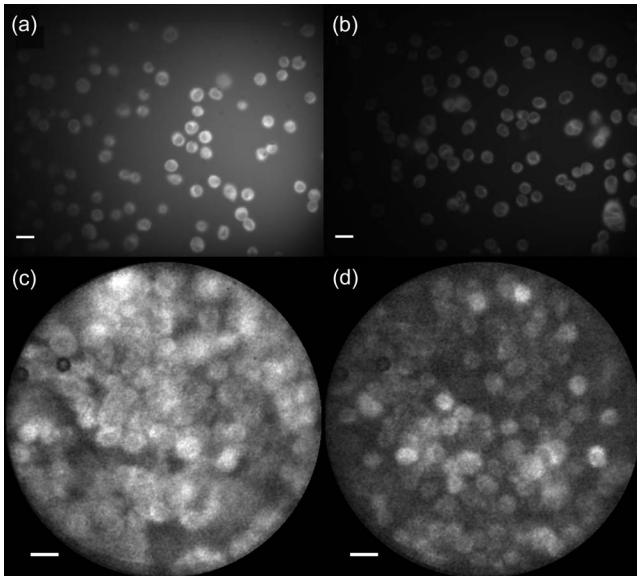


**Fig. 3** Cultured cervical cancer cells (SiHa) stained with 1% CV. Images (a) and (b) are from a bench-top wide-field fluorescence microscope; images (c) and (d) are from the confocal microendoscope. In images (a) and (c), the stain is not adjusted (native pH is 3.5); in images (b) and (d), the stain is adjusted to a physiological pH of 7.2. The fluorescence intensity is lower in adjusted-pH stain; however, the cells can still be clearly delineated. Scale bars are 20  $\mu\text{m}$ .

cause the lesions were typically small and located in a bifurcation, precise biopsy of the exact same sites could be readily accomplished. The remaining part of the procedure included the acquisition of biopsies from the same sites where confocal images had been taken.

Although the confocal probe was only 1.25 mm in diameter, two bronchoscopes were used because the length of the lens tube at the tip of the probe (10 mm) and its square leading edge made it difficult to navigate the initial bend of the BF-40's instrument channel with a 2.2-mm diameter compared to the 3.2-mm-diam channel of the BF-XT40. However, the autofluorescence image quality of the BF40 was superior to the BF-XT40. Consequently, following the confocal imaging procedure, the bronchoscope was changed back to the BF40 for precise biopsy of the sites of interest. The CV did not appear to distort the autofluorescence signal.

### 3 Results

#### 3.1 Cultured Cells and Staining Protocol

The results of SiHa cells stained with native 1% CV (pH 3.5) and CV with a pH adjusted to 7.2 are shown in Figs. 3(a)–3(d). Images A and B were acquired using a bench-top wide-field fluorescence microscope, while images C and D were acquired using the confocal microendoscope. The scale bars are 20  $\mu\text{m}$ . A control sample that was not stained with CV (not shown) did not show any fluorescence. The average cellular fluorescence for the native [Figs. 3(a) and 3(c)] and pH-adjusted [Figs. 3(b) and 3(d)] cases was measured by calculating an average intensity from the cells in images A and B. The mean fluorescence of cells stained with native CV was 172.1 gray levels ( $\sigma=5.8$ ,  $N=54$  cells), while that of the cells stained with pH-adjusted CV was 68.2 gray levels ( $\sigma=4.8$ ,

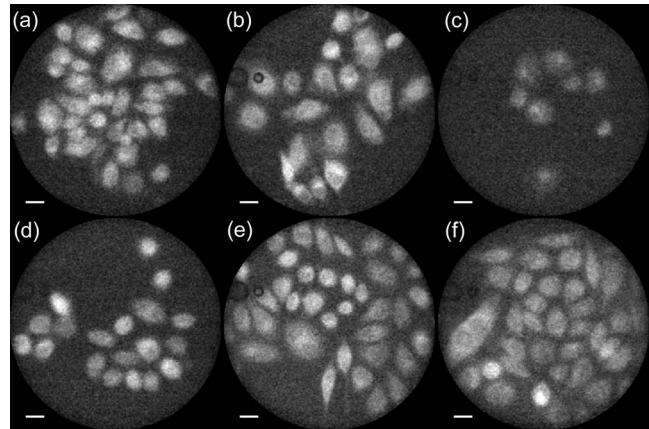


**Fig. 4** Cultured NHBE cells stained with pH-adjusted 1% CV. Staining time for images (a) through (f) is 4, 8, 16, 30, 60, and 120 s, respectively. The CV stain was taken up rapidly and persisted through to at least 120 s. The stain appears to be taken up by the cytoplasm. In image (f), one can clearly see the darker nuclei in the left-most cells. Images were acquired using the confocal microendoscope. Scale bars are 20  $\mu\text{m}$ .

$N=60$  cells). The pH adjustment decreased the intensity of cellular fluorescence by a factor of  $2.5 \pm 0.2$ . This reduced intensity is apparent in Figs. 3(b) and 3(d).

The time series of images acquired with the confocal microendoscope used to assess uptake of the CV stain is illustrated in Fig. 4. The figure shows cultured NHBE cells stained with 1% CV and a pH adjusted to 7.2. Staining time for images A through F is 4, 8, 16, 30, 60, and 120 s, respectively. Scale bars are 20  $\mu\text{m}$ . The CV stain was taken up rapidly and persisted through to at least 120 s. The stain appears to be taken up by the cytoplasm. In image F, one can clearly see the darker nuclei in the left-most cells.

#### 3.2 Ex Vivo Imaging of Bronchial Biopsy Specimens

Correlations of confocal images of the biopsy specimens with the histopathology are presented here for hyperplasia, mild, moderate, and severe dysplasia, and glandular carcinoma. Initial images (Fig. 5) were acquired from specimens stained with CV of native pH using the bench-top system to verify feasibility of the staining protocol and for comparison with pH-adjusted CV. All subsequent imaging (Figs. 6–8) was performed using the pH-adjusted stain. All images are scaled for identical magnification, and the scale bars are 20  $\mu\text{m}$ .

H&E stained sections and corresponding bench-top confocal fluorescence images of the biopsy specimens are shown in Fig. 5. Cellular and architectural features are clearly visible in the confocal images. The specimens were stained with 1% CV (native pH) prior to confocal imaging. The specimen imaged in the top half of the figure was excised from the right lower lobe bronchus (RB7). Histopathology (A) indicates hyperplasia (normal). The corresponding confocal images are shown in Figs. 5(b) and 5(c). The lower half of the figure was from the left upper lobe. The H&E image in Fig. 5(d) indicates moderate dysplasia. The corresponding confocal images are shown in Figs. 5(e) and 5(f). The cells in Figs. 5(e) and 5(f) (moderate dysplasia) are larger than those in Figs. 5(b) and 5(c) (hyperplasia).

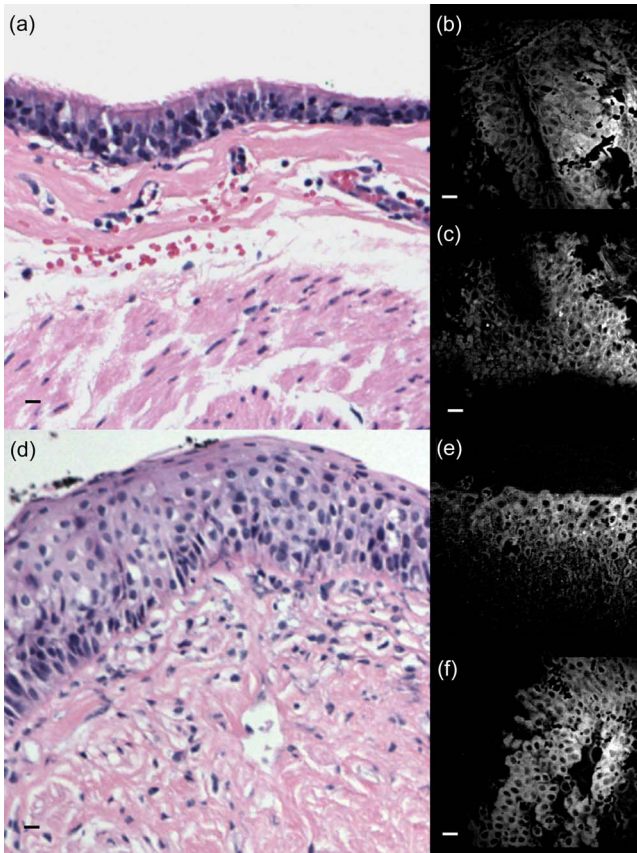


**Fig. 5** Histology (H&E sections) and corresponding confocal fluorescence images (1% CV, native pH) of bronchial biopsy specimens acquired with the bench-top microscope. Section (a) indicates hyperplasia (normal) with corresponding confocal images (b) and (c). Section (d) indicates moderate dysplasia with corresponding confocal images (e) and (f). Cellular and architectural features are clearly visible in the confocal images. Scale bars are 20  $\mu\text{m}$ .

The histopathology (mild dysplasia, severe dysplasia, invasive glandular carcinoma) and the corresponding (*ex vivo*) confocal microendoscopy images are shown in Figs. 6–8. The confocal images in Figs. 6(b)–6(f) are from different fields of view from the same specimen and have been refocused to optimize image contrast. Compared to the normal cells in Fig. 4, the tumor cells are larger with angulated nuclei. The larger glandular structures in image B (stars) may correspond to those in the H&E section. Smaller glandular structures with a larger cellular component are marked in image F (arrows). Figures 7 and 8 are from areas with mild and severe dysplasia, respectively. Individual cells are resolvable as the dark nuclear areas (arrows), where the nucleus-to-nucleus separation is sufficiently large. The extra cellular space between adjacent cells (cell borders) is visible in the bench-top confocal image of Fig. 7(f), which has higher intrinsic resolution. Although the cellular features are different from normal and invasive carcinoma in Figs. 4 and 6, respectively, it was not possible to distinguish with certainty severe versus mild dysplasia from the confocal microendoscopy images.

### 3.3 In Vivo Imaging

The confocal microendoscope was tested *in vivo* on five

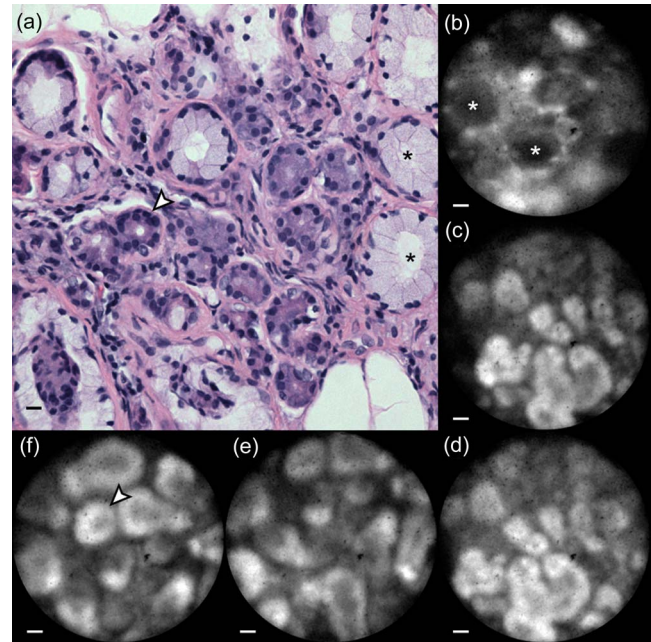


**Fig. 6** Histology [H&E stained section, (a)] indicating glandular carcinoma and corresponding confocal microendoscopy images (b)–(f) acquired *ex vivo* from a bronchial biopsy specimen. The larger glandular structures in image (b) (stars) may correspond to those in the H&E section (stars). Smaller glandular structures with a larger cellular component are marked in image (f) (arrows). Images are scaled for identical magnification. Scale bars are 20  $\mu\text{m}$ .

heavy smokers during autofluorescence bronchoscopy. Confocal imaging data was acquired and processed at a single site of interest in four patients (data for one of the five patients was lost due to a hard disk failure).

The histopathology and confocal microendoscopic images from two of the four cases are presented in Fig. 9. The H&E stained section (A) showed hyperplasia (normal). Images B–E are from different fields of view acquired at the same site (main carina). Individual cells with good localization of CV dye (dark nuclei) are identified by the arrows in images B and E. Unlike the nonhomogeneous tissue architecture illustrated in Figs. 7 and 8 for mild and moderate dysplasia, the uniformly distributed field of cells shown in Fig. 9 is consistent with normal epithelium. Image F shows a frame acquired from a different patient and site for comparison. Pathological examination at this site (right upper lobe) also showed hyperplasia (data not shown). The best images were acquired when the confocal probe was directly perpendicular to the tissue, as was the case for the main carina illustrated in B–E. Video of the confocal microendoscopy acquired *in vivo* from the main carina is shown in Video 1.

## 4 Discussion

### 4.1 CV Staining Protocol

Our initial CV staining protocol was based on a study by George and Meining.<sup>11</sup> They tested various concentrations of CV in PBS on freshly resected samples of swine esophageal and gastric mucosa using confocal microscopy. After 2 min mucolysis with acetylcysteine, the CV solution was applied

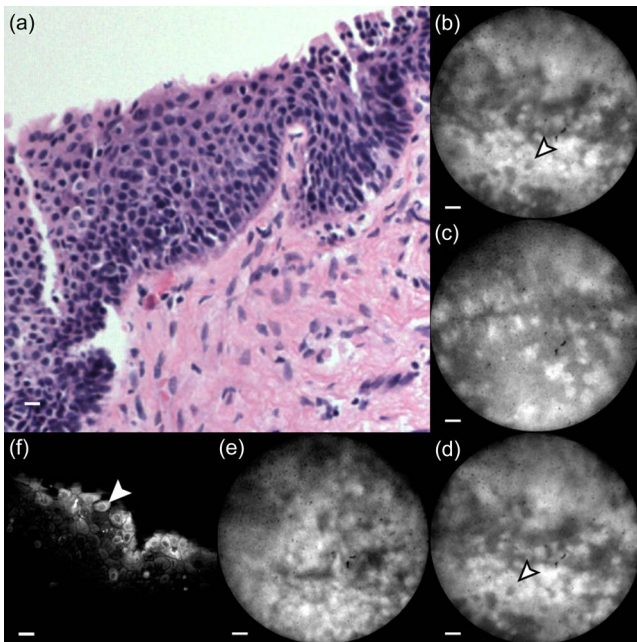


**Fig. 7** Histology [H&E stained section, (a)] indicating mild dysplasia and corresponding confocal microendoscopy (b)–(e) and bench-top confocal (f) images acquired *ex vivo* from a biopsy specimen. Individual cells are resolvable (arrow) where the nucleus-to-nucleus separation is sufficiently large. Images are scaled for identical magnification. Scale bars are 20  $\mu\text{m}$ .

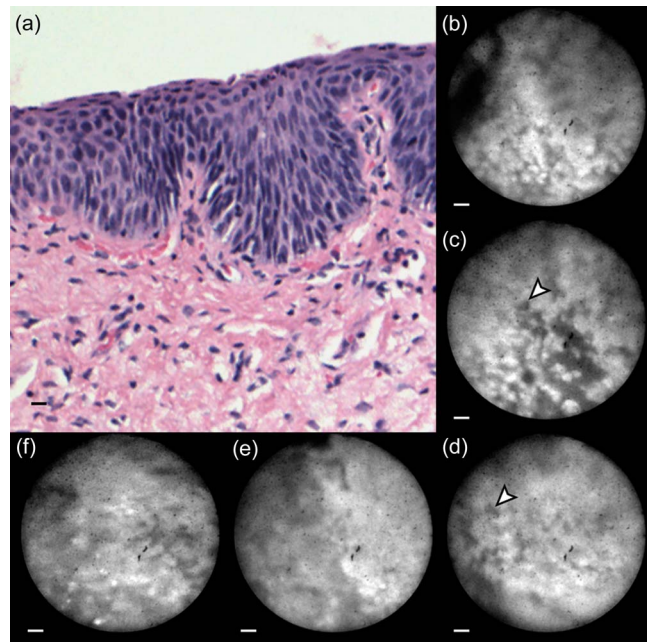
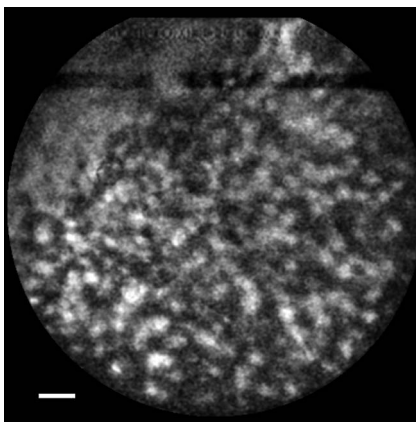


**Fig. 8** Histology [H&E stained section, (a)] indicating severe dysplasia and corresponding confocal microendoscopy images (b)–(f) acquired *ex vivo* from a bronchial biopsy. Individual cells are resolvable (arrows) where the nucleus-to-nucleus separation is sufficiently large. Images are scaled for identical magnification. Scale bars are 20  $\mu\text{m}$ .

typically for 2 min. The authors reported that a 2% (w/v) solution provided the best identification and differentiation of nuclei, membranes, and cytoplasm.

In our study, we used a 1% (w/v) solution of CV in PBS. We were unable to use a 2% solution because we observed small granules of CV in the cell culture images at this concentration. The CV granules were 5–50  $\mu\text{m}$  in size and absorbed light strongly but emitted no fluorescence. Because the stain solution was filtered to remove any undissolved solute before it was applied to the cell culture, the solubility of the stain may have changed due to the cellular environment.



**Video 1** Confocal microendoscopy video acquired *in vivo* from the main carina. (Quicktime 1.5 MB)  
[URL: <http://dx.doi.org/10.1117/1.3103583.1>]

The pH of the CV stain was adjusted from its native pH of 3.5–7.2, because acidic fluid can potentially induce fatal non-cardiogenic pulmonary edema in humans. The PBS provided a buffering system to maintain the stain solution within a physiological pH range. However, the PBS had insufficient capacity to buffer its pH when the CV was added at a concentration of 1%. Because the concentration of CV exceeded the buffering capacity of the PBS, the stain was precisely neutralized to physiological pH by the addition of sodium hydroxide. Although the fluorescence was reduced by more than a factor of two from pH adjustment and the use of a lower concentration of CV, as shown by Fig. 3, it was still sufficient to capture images of sufficient quality by increasing the optical power or using a longer integration time to acquire images with the same signal-to-noise ratio. The absorption and fluorescence maxima of CV in water are 586 and 631 nm, respectively.<sup>27</sup> We used a diode-pumped solid-state laser at 561 nm for excitation. The reduction in fluorescence intensity in cultured cells is probably a direct consequence of the increased pH modifying the electron configuration of the CV cation. We used SiHa cells that were readily available in our laboratory to test the fluorescence yield at physiological pH prior to the *in vivo* study in humans. Sufficient fluorescence was confirmed in the *in vivo* studies similar to our *ex vivo* study.

#### 4.2 Imaging of Cultured Cells

We initially used SiHa cells that were readily available in our laboratory to test the fluorescence yield of CV at physiological pH prior to the *in vivo* study in humans. Subsequently, we

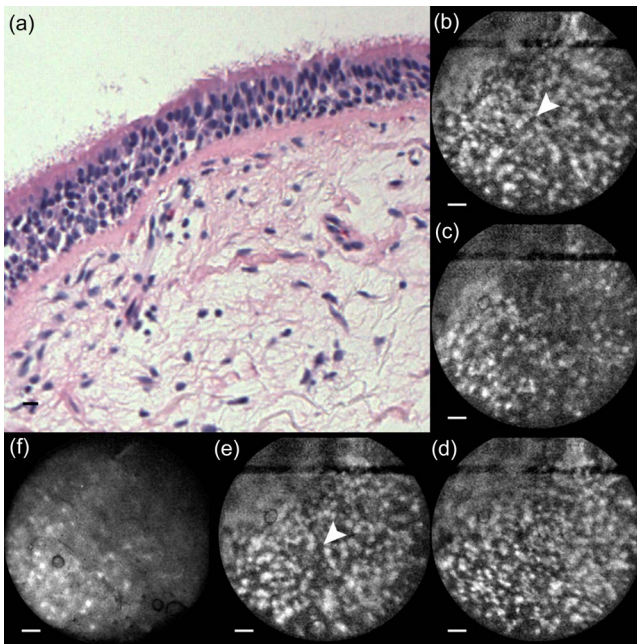


**Fig. 9** Histology [H&E stained section, (a)] indicating hyperplasia and corresponding confocal microendoscopy images (b)–(e) acquired *in vivo* from the main carina. Individual cells with good localization of CV dye (dark nuclei) are identified by the arrows in images (b) and (e). The uniformly distributed field of cells is consistent with normal epithelium. Image (f) is from a different patient and site (right upper lung). Pathology (not shown) at this site also indicated hyperplasia. Images are scaled for identical magnification. Scale bars are 20  $\mu\text{m}$ .

also tested the uptake of CV in NHBE cells (Fig. 4). The CV stain was found to be taken up by NHBE cells very quickly, similar to the tumor cells. The wide-field fluorescence images [Figs. 3(a) and 3(b)] and the confocal microendoscopic images (Figs. 3(c), 3(d), and 4) of cultured cells verify the potential of CV as fluorescent stain. These images show that the center of the cells are darker than the periphery (less fluorescence in the center), suggesting that the CV stain is accumulating in the cytoplasm of the cells.

#### 4.3 *Ex vivo* Imaging of Bronchial Biopsy Specimens

We acquired two biopsies per site so that one specimen could be used for histopathology and the other stained with CV and used for confocal microscopy. Because CV acetate is a water-soluble stain, it should have been removed during the dehydration steps of the H&E staining protocol. The samples that were stained with CV and then subsequently stained for histopathology did not show any noticeable difference when observed by an experienced lung pathologist.

Similar to the cell culture experiments (Figs. 3 and 4), the bench-top confocal images of bronchial biopsy specimens in Fig. 5 also suggest that CV accumulates in the cytoplasm of cells and not the nuclei. George and Meining used a similar protocol with a 2% (w/v) CV stain in PBS and reported that the CV led to the identification of nuclei and cell membranes.<sup>11</sup> In its neurobiological application, CV has an affinity for basophilic structures (such as nuclei and Nissl

bodies) in fixed tissue sections examined under bright-field<sup>28</sup> and, more recently, fluorescence microscopy.<sup>29</sup> These discrepancies may be due to a number of factors. First, the tissue types are different in each case—human bronchial tissue in this work, swine esophageal and gastric tissue in the work by George and Meining, and neuronal tissue in the case of Nissl staining. Second, Nissl staining is used to stain fixed specimens and not as a vital stain, as reported here and by George and Meining. Third, and probably most importantly, the pH of the stain used in this study was neutral, while in the other cases it was acidic. The binding of dye molecules is dependent on the physical–chemical properties of the stain, tissue components, solvent (including additives), and pH.<sup>30</sup> Solvent pH determines the electrical charge configuration of dye molecules, and this in turn drives their selectivity and affinity for biological molecules in tissue. The differences observed in the accumulation of dye between this study and the study by George and Meining may therefore be principally due to the difference in pH.

The images in Figs. 5(b), 5(c), 5(e), and 5(f) have sufficient nuclear-cytoplasmic contrast for quantitative cell morphology (calculation of nuclear-to-cytoplasmic ratio, for example) and the quantitative analysis of tissue architecture. As seen qualitatively in the figure, the cells in images E and F (moderate dysplasia) are much larger than those in images B and C (hyperplasia). Although architectural features were not calculated here, it was recently reported in fresh cervical samples that the mean cell separation can discriminate normal tissue from high-grade precancerous lesion using confocal microscopy.<sup>31</sup> Comparison of the microendoscopy images in Figs. 7(b)–7(d) with the bench-top confocal microscope image [Fig. 7(f)] shows that further improvement in microendoscopy is needed to achieve better image quality that is sufficient for classification of preneoplastic lesions.

#### 4.4 *In Vivo* Imaging of Bronchial Epithelium

Figure 9 illustrates some of the issues with confocal microendoscopy. When the confocal probe is placed directly perpendicular to the bronchial surface with minimal movement artifact, [Figs. 9(b)–9(e), main carina], individual cells can be clearly seen. However, the image quality becomes worse when the probe is placed at an angle (Fig. 9(f) right upper lobe). Even though significant care was taken to acquire *en face* images of the bronchial biopsy samples, these small tissue specimens warp and shrink after removal, resulting in related distortions in the acquired images.

Figure 9 included an image (F) from a different patient and site to show that the technique is repeatable. In practice, it was technically challenging to acquire good-quality images (high contrast with no motion artifacts) at the microscopic level due to motion of the confocal probe from respiratory movement and cardiac pulsation. In addition, because the probe's objective lens has a fixed working distance, and the thickness of the epithelium can vary considerably, it is possible that in cases where few cells were visible, it was because the probe was imaging at different levels of the epithelium where the cell density is different. It is also possible that some of the cells were scraped off the basement membrane in the process of positioning the probe precisely over the site of interest.

The resolution and degree of confocality in our system could be improved if the objective lens was corrected for axial chromatic aberration. This system was originally designed with a GRIN objective for reflectance-mode imaging, where axial chromatic aberrations are not important. The axial chromatic aberration caused the emission focus to be  $\sim 10\text{-}\mu\text{m}$  deeper into the tissue than the absorption (excitation) focus. As a result, a large detection pinhole was required to achieve adequate signal-to-noise ratio, and consequently, the images were a mix of confocal and wide field. Nevertheless, the GRIN lens performed sufficiently. In real time, the images are better than the still images as presented here.

Other studies have reported microendoscopy of bronchial mucosa using contrast from either autofluorescence or exogenous fluorescence from methylene blue. Thiberville et al.<sup>32</sup> used the Mauna Kea instrument (Cell vizio) and autofluorescence from the basement membrane to study alterations associated with premalignant bronchial lesions *in vivo*. These researchers observed decreased autofluorescence and increased disorganization in the subepithelial network of structural proteins (primarily elastin) in metaplastic, dysplastic, and cancerous lesions as compared with normal sites. This is consistent with the findings of autofluorescence bronchoscopy.<sup>8</sup> Similar to our experience, the epithelial cells could not be visualized without an exogenous dye. The same researchers have gone on to use an exogenous dye (methylene blue) to provide cellular contrast in the bronchial epithelium.<sup>33</sup> Further studies are required to compare different dyes for *in vivo* imaging.

## 5 Conclusions

We reported results here from a pilot study of five patients who were recruited from two ongoing NIH/National Cancer Institute sponsored lung-cancer chemoprevention trials. Using a laser-scanning engine and a bronchoscope-compatible fiber-optic confocal probe with a GRIN objective lens as well as a neutral pH CV staining protocol, sufficient contrast was observed to identify tissue morphology that can distinguish normal cells from tumor cells. Correction of the chromic aberration in the distal lens is required to fully realize the potential of this technique as a noninvasive imaging tool to study the natural history of preneoplastic lesions. Refinements to the instrumentation are ongoing and will be reported in subsequent contributions.

## Acknowledgments

This study was supported in part by grants from the National Institutes of Health (No. 5-P01-CA096964-02, No. U01-CA96109, and No. 1R01 CA10383) and the National Cancer Institute of Canada (Grant No. 12067). We thank Jogoda Korbelik and Anita Carraro for preparation of the CV stains and Priscilla Fung for preparation of the cell cultures.

## References

1. A. Jemal, R. Siegel, E. Ward, T. Murray, J. Q. Xu, and M. J. Thun, "Cancer statistics, 2007," *Ca-Cancer J. Clin.* **57**(1), 43–66 (2007).
2. H. G. Welch, L. M. Schwartz, and S. Woloshin, "Are increasing 5-year survival rates evidence of success against cancer?," *JAMA, J. Am. Med. Assoc.* **283**(22), 2975–2978 (2000).

3. L. Z. Tong, M. R. Spitz, J. J. Fueger, and C. I. Amos, "Lung carcinoma in former smokers," *Cancer* **78**(5), 1004–1010 (1996).
4. W. K. Hong and M. B. Sporn, "Recent advances in chemoprevention of cancer," *Science* **278**(5340), 1073–1077 (1997).
5. S. Lam, J. C. LeRiche, Y. Zheng, A. Coldman, C. MacAulay, E. Hawk, G. Kelloff, and A. F. Gazdar, "Sex-related differences in bronchial epithelial changes associated with tobacco smoking," *J. Natl. Cancer Inst.* **91**(8), 691–696 (1999).
6. S. Bota, J. B. Auliac, C. Paris, J. Metayer, R. Sesboue, G. Nouvet, and L. Thiberville, "Follow-up of bronchial precancerous lesions and carcinoma *in situ* using fluorescence endoscopy," *Am. J. Respir. Crit. Care Med.* **164**(9), 1688–1693 (2001).
7. L. B. Woolner, "Pathology of cancer detected cytologically," in *Atlas of Early Lung Cancer*, National Cancer Institute, Ed., pp. 107–213, Igaku-Shoin, New York (1983).
8. S. Lam, C. MacAulay, J. C. LeRiche, and B. Palcic, "Detection and localization of early lung cancer by fluorescence bronchoscopy," *Cancer* **89**(11), 2468–2473 (2000).
9. I. W. Park, I. I. Wistuba, A. Maitra, S. Milchgrub, A. K. Virmani, J. D. Minna, and A. F. Gazdar, "Multiple clonal abnormalities in the bronchial epithelium of patients with lung cancer," *J. Natl. Cancer Inst.* **91**(21), 1863–1868 (1999).
10. S. Kudo, C. A. Rubio, C. R. Teixeira, H. Kashida, and E. Kogure, "Pit pattern in colorectal neoplasia: endoscopic magnifying view," *Endoscopy* **33**(4), 367–373 (2001).
11. M. George and A. Meining, "Cresyl violet as a fluorophore in confocal laser scanning microscopy for future *in vivo* histopathology," *Endoscopy* **35**(7), 585–589 (2003).
12. A. Meining, D. Saur, M. Bajbouj, V. Becker, E. Peltier, H. Hoefler, C. H. Von Weyhern, R. M. Schmid, and C. Prinz, "In vivo histopathology for detection of gastrointestinal neoplasia with a portable, confocal miniprobe: an examiner blinded analysis," *Clin. Gastroenterol. Hepatol.* **5**(11), 1261–1267 (2007).
13. L. J. Hornbeck, "Digital light processing for high-brightness, high-resolution applications," *Proc. SPIE* **3013**, 27–40 (1997).
14. P. Lane, A. Dlugan, and C. MacAulay, "DMD-enabled confocal microendoscopy," *Proc. SPIE* **4251**, 192–198 (2001).
15. C. MacAulay and A. Dlugan, "Use of digital micro mirror devices in quantitative microscopy," *Proc. SPIE* **3260**, 201–206 (1998).
16. S. Lam, B. Standish, C. Baldwin, A. McWilliams, J. LeRiche, A. Gazdar, A. I. Vitkin, V. Yang, N. Ikeda, and C. MacAulay, "In vivo optical coherence tomography imaging of preinvasive bronchial lesions," *Clin. Cancer Res.* **14**(7), 2006–2011 (2008).
17. P. L. Hsiung, P. R. Nambiar, and J. G. Fujimoto, "Effect of tissue preservation on imaging using ultrahigh resolution optical coherence tomography," *J. Biomed. Opt.* **10**(6), 064033 (2005).
18. N. S. Goldstein, A. Soman, and J. Sacksner, "Disparate surgical margin lengths of colorectal resection specimens between *in vivo* and *in vitro* measurements—the effects of surgical resection and formalin fixation on organ shrinkage," *Am. J. Clin. Pathol.* **111**(3), 349–351 (1999).
19. C. MacAulay, P. Lane, and R. Richards-Kortum, "In vivo pathology: microendoscopy as a new endoscopic imaging modality," *Gastrointest Endosc. Clin. N. Am.* **14**(3), 595–620 (2004).
20. A. F. Gmitro and D. Aziz, "Confocal microscopy through a fiberoptic imaging bundle," *Opt. Lett.* **18**(8), 565–567 (1993).
21. K. B. Sung, C. Liang, M. Descour, T. Collier, M. Follen, A. Malpica, and R. Richards-Kortum, "Near real time *in vivo* fibre optic confocal microscopy: subcellular structure resolved," *J. Microsc.* **208**, 75–75 (2002).
22. D. L. Dickensheets and G. S. Kino, "Micromachined scanning confocal optical microscope," *Opt. Lett.* **21**(10), 764–766 (1996).
23. P.-M. Delaney, M. R. Harris, and R. G. King, "Novel microscopy using fiber optic confocal imaging and its suitability for subsurface blood-vessel imaging *in vivo*," *Clin. Exp. Pharmacol. Physiol.* **20**(3), 197–198 (1993).
24. J. Knittel, L. Schnieder, G. Buess, B. Messerschmidt, and T. Possner, "Endoscope-compatible confocal microscope using a gradient index lens system," *Opt. Commun.* **188**(5–6), 267–273 (2001).
25. P. M. Lane, R. P. Elliott, and C. E. MacAulay, "Confocal microendoscopy with chromatic sectioning," *Proc. SPIE* **4959**, 23–26 (2003).
26. S. Lam, T. Kennedy, M. Unger, Y. E. Miller, D. Gelmont, V. Rusch, B. Gipe, D. Howard, J. C. LeRiche, A. Coldman, and A. F. Gazdar, "Localization of bronchial intraepithelial neoplastic lesions by fluorescence bronchoscopy," *Chest* **113**(3), 696–702 (1998).

27. D. I. Kreller and P. V. Kamat, "Photochemistry of sensitizing dyes—spectroscopic and redox properties of cresyl violet," *J. Phys. Chem.* **95**(11), 4406–4410 (1991).
28. R. W. Horobin, "Oxazines and related dyes," in *Conn's Biological Stains: A Handbook of Dyes, Stains and Fluorochromes For Use in Biology and Medicine*, R. W. Horobin and J. A. Kiernan, Eds., pp. 281–282, BIOS, Oxford (2002).
29. A. Alvarez-Buylla, C. Y. Ling, and J. R. Kirn, "Cresyl violet—a red fluorescent nissl stain," *J. Neurosci. Methods* **33**(2–3), 129–133 (1990).
30. P. Prento, "A contribution to the theory of biological staining based on the principles for structural organization of biological macromolecules," *Biotech. Histochem.* **76**(3), 137–161 (2001).
31. T. Collier, M. Guillaud, M. Follen, A. Malpica, and R. Richards-Kortum, "Real-time reflectance confocal microscopy: comparison of two-dimensional images and three-dimensional image stacks for detection of cervical precancer," *J. Biomed. Opt.* **12**(2), 024021 (2007).
32. L. Thiberville, S. Moreno-Swirc, T. Vercauteren, E. Peltier, C. Cave, and G. B. Heckly, "*In vivo* imaging of the bronchial wall microstructure using fibered confocal fluorescence microscopy," *Am. J. Respir. Crit. Care Med.* **175**(1), 22–31 (2007).
33. L. Thiberville, M. Salaun, S. Moreno-Swirc, and G. Bourg-Heckly, "*In vivo* endoscopic microimaging of the bronchial epithelial layer using 660 nm fibered confocal fluorescence microscopy and topical methylene blue," in European Respiratory Society Annual Congress, Stockholm (2007).